The Astrophysical Journal Letters, 936:L10 (12pp), 2022 September 1 https://doi.org/10.3847/2041-8213/ac85ad

Long-duration Gamma-Ray Burst and Associated Kilonova Emission from Fast-spinning Black Hole–Neutron Star Mergers

Jin-Ping Zhu[1], Xiangyu Ivy Wang[2,3], Hui Sun[4], Yuan-Pei Yang[5], Zhuo Li[1,6], Rui-Chong Hu[7], Ying Qin[8], and Shichao Wu[9,10]

[1] Department of Astronomy, School of Physics, Peking University, Beijing 100871, People's Republic of China; zhujp@pku.edu.cn
[2] School of Astronomy and Space Science, Nanjing University, Nanjing 210093, People's Republic of China
[3] Key Laboratory of Modern Astronomy and Astrophysics (Nanjing University), Ministry of Education, People's Republic of China
[4] Key Laboratory of Space Astronomy and Technology, National Astronomical Observatories, Chinese Academy of Sciences, Beijing 100012, People's Republic of China
[5] South-Western Institute for Astronomy Research, Yunnan University, Kunming, Yunnan 650500, Peoples Republic of China; ypyang@ynu.edu.cn
[6] Kavli Institute for Astronomy and Astrophysics, Peking University, Beijing 100871, People's Republic of China; zhuo.li@pku.edu.cn
[7] Guangxi Key Laboratory for Relativistic Astrophysics, School of Physical Science and Technology, Guangxi University, Nanning 530004, People's Republic of China
[8] Department of Physics, Anhui Normal University, Wuhu, Anhui 241000, People's Republic of China
[9] Max-Planck-Institut für Gravitationsphysik (Albert-Einstein-Institut), D-30167 Hannover, Germany
[10] Leibniz Universität Hannover, D-30167 Hannover, Germany
Received 2022 June 23; revised 2022 July 28; accepted 2022 July 29; published 2022 August 29

Abstract

Gamma-ray bursts (GRBs) have been phenomenologically divided into long- and short-duration populations, generally corresponding to collapsar and compact merger origins, respectively. Here, we collect three unique bursts, GRBs 060614, 211211A, and 211227A, all of which are characterized by a long-duration main emission (ME) phase and a rebrightening extended emission (EE) phase, to study their observed properties and their potential origins as neutron star–black hole (NSBH) mergers. NS-first-born (BH-first-born) NSBH mergers tend to contain fast-spinning (nonspinning) BHs that more easily (hardly) allow tidal disruption to occur, while (without) forming electromagnetic signals. We find that NS-first-born NSBH mergers can well interpret the origins of these three GRBs, supported by the following. (1) Their X-ray MEs and EEs show unambiguous fallback accretion signatures, decreasing as $\propto t^{-5/3}$, which might account for their long durations. The EEs could result from the fallback accretion of *r*-process heating materials, which is predicted to occur after NSBH mergers. (2) The beaming-corrected local event-rate density for these types of merger-origin long-duration GRBs is $\mathcal{R}_0 \sim 2.4^{+2.3}_{-1.3}\,\mathrm{Gpc^{-3}\,yr^{-1}}$, consistent with that of NS-first-born NSBH mergers. (3) Our detailed analysis of the EE, afterglow, and kilonova of the recent high-impact event GRB 211211A reveals that it could be a merger between a $\sim 1.23^{+0.06}_{-0.07}\,M_\odot$ NS and a $\sim 8.21^{+0.77}_{-0.75}\,M_\odot$ BH, with an aligned spin of $\chi_{\rm BH} \sim 0.62^{+0.06}_{-0.07}$, supporting an NS-first-born NSBH formation channel. A long-duration burst, with a rebrightening fallback accretion signature after the ME, and a bright kilonova, might be commonly observed features for on-axis NSBH mergers. We estimate the multimessenger detection rate between gravitational waves, GRBs, and kilonova emissions from NSBH mergers in O4 (O5) to be $\sim 0.1\,\mathrm{yr^{-1}}$ ($\sim 1\,\mathrm{yr^{-1}}$).

Unified Astronomy Thesaurus concepts: Gamma-ray bursts (629); Neutron stars (1108); Black holes (162); Gravitational waves (678)

1. Introduction

In observations, a critical duration of $T_{90} \sim 2$ s is usually adopted to separate gamma-ray bursts (GRBs) into long- and short-duration populations (Norris et al. 1984; Kouveliotou et al. 1993). Long-duration GRBs (lGRBs) have been identified as originating from massive collapsars, due to their association with broadline Type Ic supernovae (e.g., Galama et al. 1998; Woosley & Bloom 2006) and their exclusive hosting in star-forming galaxies (e.g., Bloom et al. 1998; Christensen et al. 2004). It has long been suspected that neutron star mergers, including binary neutron star (BNS) and neutron star–black hole (NSBH) mergers, are the potential origins of short-duration GRBs (sGRBs; Paczynski 1986, 1991; Eichler et al. 1989; Narayan et al. 1992). Due to the natal kicks impacted on binaries at birth and the long inspiral delays before mergers, NS mergers are believed to occur in low-density environments, with significant offsets away from the centers of their host galaxies (e.g., Narayan et al. 1992; Bloom et al. 1999) being supported by observations (e.g., Fong et al. 2010, 2015; Li et al. 2016). NS mergers can release an amount of neutron-rich matter (Lattimer & Schramm 1974, 1976; Symbalisty & Schramm 1982), which allows elements heavier than iron to be synthesized via the rapid neutron-capture process (*r*-process). It was predicted that the radioactive decay of these *r*-process nuclei would power an ultraviolet–optical–infrared thermal transient named "kilonova" (Li & Paczyński 1998; Metzger et al. 2010b).

The smoking gun evidence for the BNS merger origins of sGRBs and kilonovae was the multimessenger observations of the first BNS merger gravitational-wave (GW) source GW170817, detected by the LIGO/Virgo Collaboration (LVC; Abbott et al. 2017a), and the subsequent associated electromagnetic (EM) signals, including an sGRB,

GRB 170817A, triggered by the Fermi Gamma-ray Burst Monitor (Abbott et al. 2017b; Goldstein et al. 2017; Savchenko et al. 2017; Zhang et al. 2018); a broadband jet afterglow from radio to X-ray, with an off-axis viewing angle (e.g., Margutti et al. 2017; Troja et al. 2017; Lazzati et al. 2018; Lyman et al. 2018; Lamb et al. 2019; Ghirlanda et al. 2019); and a fast-evolving kilonova transient (AT2017gfo; e.g., Abbott et al. 2017c; Arcavi et al. 2017; Coulter et al. 2017; Drout et al. 2017; Evans et al. 2017; Kasliwal et al. 2017; Kilpatrick et al. 2017; Pian et al. 2017; Smartt et al. 2017). With the confirmation of the origins of sGRBs and kilonovae from the BNS merger population, one may particularly expect to further establish the connection between NSBH mergers and their associated EM counterparts. However, although two high-confidence NSBHs (i.e., GW200105 and GW200115) and a few marginal NSBH GW candidates were detected during the third observing run of LVC (Abbott et al. 2021a; Nitz et al. 2021; the LIGO Scientific Collaboration et al. 2021), EM counterparts in the follow-up observations of these GWs were missing (e.g., Andreoni et al. 2020; Coughlin et al. 2020; Gompertz et al. 2020a; Kasliwal et al. 2020; Page et al. 2020; Anand et al. 2021), except for an amphibious association between a subthreshold GRB, GBM-190816, and a subthreshold NSBH event (Goldstein et al. 2019; Yang et al. 2020). One plausible explanation for the lack of detection of EM counterparts is that present EM searches are too shallow to achieve the distance and volumetric coverage for the probability maps of LVC events (Coughlin et al. 2020; Sagués Carracedo et al. 2021; Zhu et al. 2021b). Furthermore, detailed studies on these NSBH candidates (Zhu et al. 2021a, 2022; Fragione 2021; Mandel & Smith 2021; D'Orazio et al. 2022; Gompertz et al. 2022a) revealed that they were more likely to be plunging events, and could hardly produce any bright EM signals, owing to the near-zero spins of the primary BHs, since NSBH mergers tend to make tidal disruptions and drive bright EM counterparts if the primary BHs have high aligned spins (e.g., Kyutoku et al. 2015; Foucart et al. 2018; Zhu et al. 2021a, 2022; Di Clemente et al. 2022).

Due to the lack of smoking gun evidence, it is unclear whether NSBH mergers can contribute to the sGRB population (e.g., Gompertz et al. 2020b). On the one hand, the majority of NSBH binaries are believed to originate from the classic isolated binary evolution scenario (involving a common envelope; e.g., Giacobbo & Mapelli 2018; Belczynski et al. 2020; Drozda et al. 2020; Shao & Li 2021). In this scenario, the primary BHs are usually born first, and have negligible spins, consistent with the properties of LVC NSBH candidates (Broekgaarden & Berger 2021; Zhu et al. 2021a). Conversely, if the NSs are born first, the progenitors of the BHs would be efficiently tidally spun up by the NSs in close binaries (orbital periods $\lesssim 2$ days), and finally form fast-spinning BHs (Hu et al. 2022). A fraction of these NS-first-born NSBH systems that are formed in close binaries can merge within Hubble time. Therefore, compared with BH-first-born NSBH mergers, NS-first-born NSBH mergers allow tidal disruption to happen more easily and drive bright GRB emissions. Because NS-first-born NSBH mergers may only account for $\lesssim$20% of NSBH populations (Chattopadhyay et al. 2021, 2022; Román-Garza et al. 2021), GRB populations contributed from NSBH mergers should be limited. On the other hand, most disrupted NSBH mergers can eject a lot more materials and lead to more powerful fallback accretions than BNS mergers (Rosswog 2007; Fernández et al. 2017). Furthermore, *r*-process heating might affect the fallback accretion of marginally bound matter (Metzger et al. 2010a). A late-time fallback accretion of these materials may happen after tens of seconds of the merger, if the remnant BH has a mass of $\gtrsim 6-8\,M_{\odot}$. Because most NSBH mergers can remain as BHs with masses in this range, Desai et al. (2019) have suggested that an extended emission (EE) caused by the fallback accretion of *r*-process heating materials can be an important signal for distinguishing NSBH GRBs from BNS GRBs. Thus, it is plausible that the energy budgets, durations, and other observed properties of NSBH GRBs could differ from those of BNS mergers.

Very recently, observations of an lGRB (i.e., GRB 211211A) associated with a kilonova emission at a redshift $z = 0.0763$ (luminosity distance $D_{\rm L} \approx 350$ Mpc) were reported by a few groups (Chang et al. 2022; Gompertz et al. 2022b; Mei et al. 2022; Rastinejad et al. 2022; Xiao et al. 2022; Yang et al. 2022; Zhang et al. 2022). The burst was characterized by a spiky main emission (ME) phase, with a duration of $\sim$13 s, an EE phase lasting $\sim$55 s, and a temporal lull between these two phases. Since the observation property of the associated kilonova emission was similar to that of AT2017gfo[11] (Rastinejad et al. 2022; Xiao et al. 2022), indicating the origin of a compact binary coalescence, it was a challenge to interpret the intrinsically long duration of the burst. Yang et al. (2022) proposed that the merger of a near-equal-mass NS–white-dwarf binary could well explain the ME of GRB 211211A, since the accretion of some high–angular momentum white-dwarf debris onto the remnant NS could prolong the burst duration. Gao et al. (2022) suggested that a strong magnetic flux may surround the central engine of GRB 211211A, resulting in a long-duration accretion process, due to the magnetic barrier effect (Proga & Zhang 2006; Liu et al. 2012).

Besides GRB 211211A, two other redshift-known (*z*-known) lGRBs, i.e., GRB 060614 and GRB 211227A, have been proposed as deriving from compact binary coalescences. GRB 060614 (Della Valle et al. 2006; Gal-Yam et al. 2006; Zhang et al. 2007) was found to be associated with a kilonova candidate (Yang et al. 2015), while GRB 211227A showed a large physical offset from the host center and lacked the supernova signature that should have been observed at the location of the burst (Lü et al. 2022). In this *Letter*, we study the properties of these three merger-origin lGRBs, especially those of GRB 211211A, and show that a single explosive population via the NS-first-born NSBH merger could account for their origin. Here, the cosmological parameters are taken as $H_0 = 67.4\,{\rm km\,s^{-1}\,Mpc^{-1}}$, $\Omega_{\rm m} = 0.315$, and $\Omega_{\Lambda} = 0.685$ (Planck Collaboration et al. 2020).

2. Properties of Merger-origin LGRBs

2.1. Observed Properties and X-Ray Fallback Accretion Signals

We collect the observed data of three present *z*-known merger-origin lGRBs, including GRB 211221A (e.g., Rastinejad et al. 2022; Xiao et al. 2022; Yang et al. 2022), GRB 060614

[11] Waxman et al. (2022) suggested that the burst could have happened in another spatially nearby galaxy at a higher redshift. The near-infrared emission following GRB 211211A could be thermal emission from dust, heated by UV radiation produced by the interaction between the jet plasma and the circumstellar medium, rather than a kilonova emission.

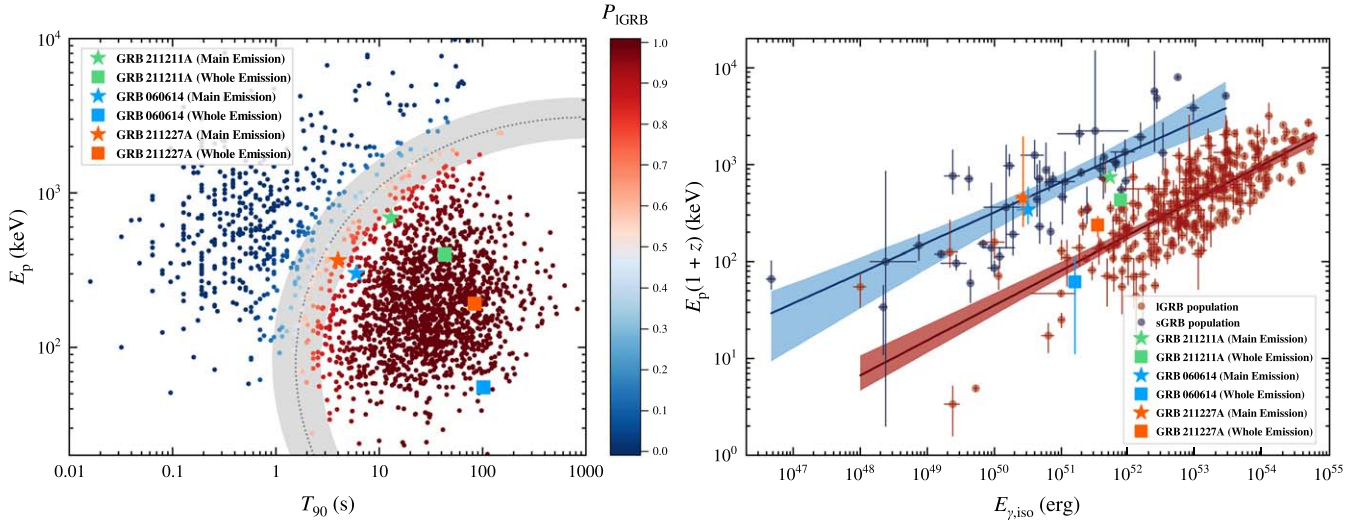

Figure 1. Left: lGRB/sGRB classification diagram in the T_{90}–$E_{\rm p}$ domain (Gruber et al. 2014; von Kienlin et al. 2014; Narayana Bhat et al. 2016; von Kienlin et al. 2020). The dashed line and the gray shaded region are the best-fit and 1σ credible boundaries for distinguishing lGRBs from sGRBs, respectively. The redder (bluer) the color of the point, the higher the possibility of the lGRB (sGRB) origin. Right: $E_{\rm p}(1+z)$ and $E_{\gamma,\rm iso}$ correlation diagram with known redshift data (Amati et al. 2002; Zhang et al. 2009; Minaev & Pozanenko 2020). The solid red and blue lines represent the best-fit correlations for lGRBs and sGRBs, respectively. The green, blue, and orange stars (squares) in both panels represent the placement of the MEs (WEs) for GRB 211211A, GRB 060614, and GRB 211227A, respectively.

Table 1
The Observed Properties Of GRB 211211A, GRB 060614,[a] and GRB 211227A[b]

	GRB 211211A	GRB 060614	GRB 211227A
ME			
Duration (s)	13	6	4
Peak energy (keV)	687^{+13}_{-11}	300^{+210}_{-90}	400^{+1200}_{-200}
Energy fluence (erg cm^{-2})	$3.77^{+0.01}_{-0.01}\times10^{-4}$	$8.2^{+0.6}_{-2.5}\times10^{-6}$	$2.01^{+0.19}_{-0.42}\times10^{-6}$
Isotropic equivalent energy (erg)	$5.30^{+0.01}_{-0.01}\times10^{51}$	$3.18^{+0.22}_{-0.98}\times10^{50}$	$2.69^{+0.25}_{-0.56}\times10^{50}$
Spectral index α	$-0.996^{+0.005}_{-0.005}$	$-1.57^{+0.12}_{-0.14}$	$-1.56^{+0.15}_{-0.06}$
Spectral index β	$-2.36^{+0.02}_{-0.02}$	…	…
WE			
Duration (s)	$43.18^{+0.06}_{-0.06}$	102 ± 5	84
Peak energy (keV)	399^{+14}_{-16}	$10-100$	192^{+45}_{-42}
Energy fluence[c] (erg cm^{-2})	$5.42^{+0.08}_{-0.08}\times10^{-4}$	$4.09^{+0.18}_{-0.34}\times10^{-5}$	$2.60^{+0.21}_{-0.21}\times10^{-5}$
Isotropic equivalent energy (erg)	$7.61^{+0.11}_{-0.11}\times10^{51}$	$1.59^{+0.07}_{-0.13}\times10^{51}$	$3.48^{+0.16}_{-0.16}\times10^{51}$
Spectral index α	$-1.20^{+0.01}_{-0.01}$	…	$-1.34^{+0.10}_{-0.08}$
Spectral index β	$-2.05^{+0.02}_{-0.02}$	…	$-2.26^{+0.24}_{-1.11}$
Redshift	0.076	0.125	0.228

Notes.
[a] The data of GRB 211221A and GRB 060614 are collected from Table 1 of Yang et al. (2022).
[b] The data of GRB 211227A are collected from Lü et al. (2022) and Tsvetkova et al. (2022).
[c] The energy fluence of the ME for GRB 211227A is calculated by the HEASoft tool (Nasa High Energy Astrophysics Science Archive Research Center (Heasarc), 2014), in the 15–1500 keV energy band.

(Della Valle et al. 2006; Gal-Yam et al. 2006; Zhang et al. 2007), and GRB 211227A (Lü et al. 2022), all characterized by a spiky long-duration ME phase, a rebrightening EE phase, and a temporal lull between these two phases, to study their similarities. Here, the EE phase is defined as the long-lasting lower-level emission phase after the initial intense ME phase (Norris & Bonnell 2006; Lan et al. 2020). The whole emission (WE) phase includes the ME phase and the EE phase. Table 1 lists the observed properties of the ME and the WE phases.

In the left panel of Figure 1, we divide the detected GRBs into two populations, i.e., lGRB and sGRB populations, in the duration T_{90} versus Earth-frame peak energy $E_{\rm p}$ diagram, through the Gaussian mixture model. The intermediate population at the boundary region between the lGRB and sGRB populations could originate from collaspars or from compact-object coalescences (e.g., Tunnicliffe & Levan 2012; Zaninoni et al. 2016). Both the MEs and WEs of these three merger-origin GRBs fall into the distribution of lGRBs. Therefore, without the redshift, host galaxy information, and associated kilonova detection, these three bursts would be classified as members of the lGRB population, due to their long durations.

The correlations between the total isotropic equivalent energy $E_{\gamma,\rm iso}$ of the prompt emission and the rest-frame peak energy $E_{\rm p}(1+z)$ (the Amati relation; Amati et al. 2002) for both the lGRB and sGRB populations are shown in the right

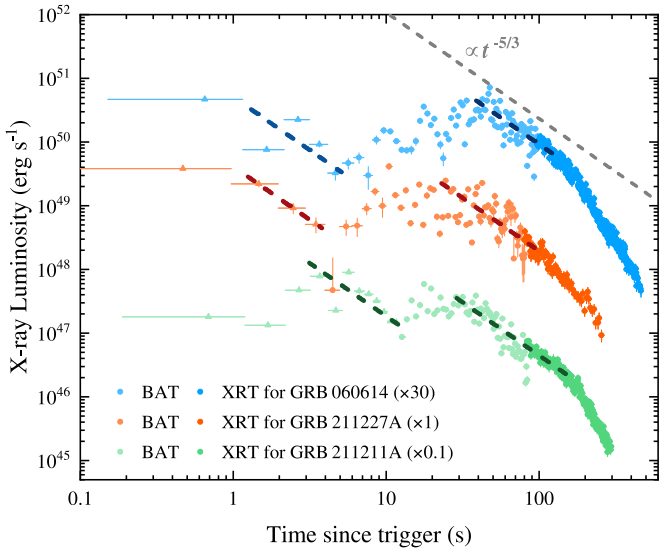

Figure 2. Burst Alert Telescope (BAT) and Swift X-Ray Telescope (XRT) light curves of GRB211211A (green), GRB060614 (blue), and GRB211227A (orange). The BAT luminosity is calculated at 10 keV. Their MEs and EEs are marked with the triangles and circles, respectively. The dashed lines represent the X-ray light curves that track the $\propto t^{-5/3}$ mass fallback accretion.

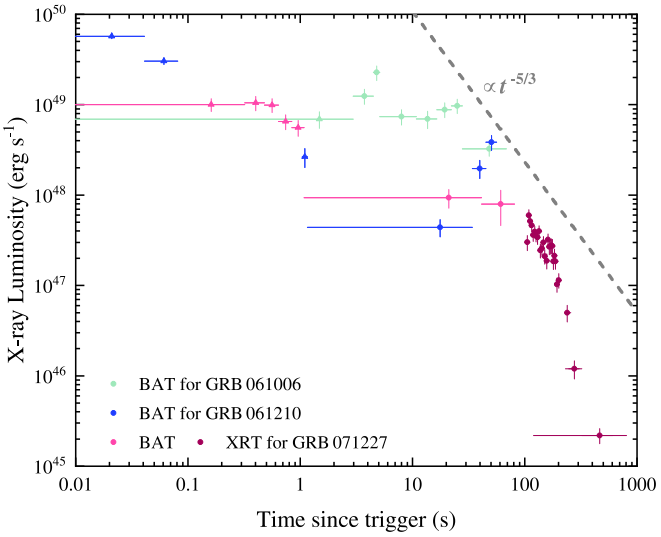

Figure 3. Similar to Figure 2, but for GRB 061006 (green), GRB 061210 (dark blue), and GRB 071227 (purple).

panel of Figure 1. We find that the WEs of these three bursts still behave as normal lGRBs, although their $E_{\gamma,\rm iso}$ are lower than those of most observed lGRBs. Conversely, their MEs lie on the middle location of the sGRB track, rather than on the lGRB track. The differences in $E_{\gamma,\rm iso}$ between the WEs and MEs, corresponding to the $E_{\gamma,\rm iso}$ of the EEs, for these bursts are similar, which are $\sim$1–2 $\times$ 10^{51} erg.

After a BNS/disrupted NSBH merger, a compact remnant accretion disk would be formed around the NS or BH. The lifetime of this disk is typically $\lesssim$1 s, which is thought to determine the burst duration of an sGRB (e.g., Shapiro 2017; Zhang 2019; Ruiz et al. 2020). In order to explain the long durations of these three merger-origin GRBs, an additional energy/matter injection is needed. When a group of bound ejecta with an energy distribution of $dM/dE \propto E^{\alpha}$, where $\alpha \approx 0$ around $E = 0$, fall back onto the central NS or BH, the fallback rate would track as $\propto t^{-5/3}$ (Rees 1988). As shown in Figure 2, we find that there are long-duration fallback accretion signals appearing in the X-ray light curves of both the MEs and EEs for these three bursts. The fallback rates in the EEs peak at $\sim$20–40 s and follow $\propto t^{-5/3}$, with a duration of $\sim$100–200 s. Thus, the fallback accretion might result in their long durations.

Gompertz et al. (2020a) collected 39 z-known sGRBs (seven events had an EE), and searched for possible NSBH candidates among these sGRBs. However, they did not find any clear evidence for the existence of NSBH GRBs in this complete sGRB sample. If a millisecond magnetar can survive after a BNS merger, the magnetar can lose its rotational energy via the spin-down process, resulting in a long-duration X-ray plateau in the X-ray light curve (Zhang & Mészáros 2001). Gompertz et al. (2020a) suggested that four of the sGRBs with EEs in their sample could be magnetar-like, so they could not originate from NSBH mergers. In Figure 3, we collect the X-ray light curves of the three other sGRBs with EEs, including GRB 061006 (Berger 2007), GRB 061210 (Berger 2007), and GRB 071227 (D'Avanzo et al. 2009), whose X-ray emissions could not be well interpreted via the magnetar model by Gompertz et al. (2020a). We find that GRB 071227 could still be magnetar-like, being characterized by a long-duration X-ray plateau. The X-ray light curves of GRB 061006 and GRB 061210 do not show any signatures of $\propto t^{-5/3}$ decay, and hence they may provide no evidence of an unambiguous fallback accretion signal, though that could be partly due to their limited data points. Thus, the EEs in the present z-known sGRBs may not be caused by the fallback accretions. The similar observed properties of merger-origin lGRBs, i.e., long durations and unambiguous rebrightening fallback accretion signals, do not present in the existing observations of the merger-origin sGRBs with/without EEs, indicating a unique origin for them.

In principle, both BNS and NSBH mergers can generate early-time fallback accretions (Rosswog 2007; Metzger et al. 2010a; Fernández et al. 2017). However, most of the disrupted NSBH mergers would eject a lot more materials and lead to more powerful fallback accretions than BNS mergers (Rosswog 2007). Furthermore, the simulations by Metzger et al. (2010a) and Desai et al. (2019) showed that r-process heating might affect the materials that are marginally gravitationally bound. The gravity of the remnants formed after BNS mergers might be too low to drag these r-process heating materials back and result in fallback accretions. However, as predicted by Desai et al. (2019), the late-time fallback accretion of these materials may occur after tens of seconds of the merger, if the remnant BH has a mass of $\gtrsim$ 6–8 $M_{\odot}$, leading to a rebrightening emission with a $t^{-5/3}$ power-law decay appearing in the X-ray light curve. The EEs of these three bursts, whose starting times and observational features are consistent with the predictions of Desai et al. (2019), may originate from the fallback accretion of r-process heating materials. We thus suspect that these three bursts are derived from NSBH mergers.

2.2. Event-rate Density

Assuming the unique merger origins of these three lGRBs, we investigate their local event-rate density by tentatively constructing their luminosity function (LF), following Sun et al. (2015, 2022). The limited number of events could lead to the large uncertainty of the LF. However, it could be plausible to make a fine evaluation by adding up the contributions of all

three events. Following Equation (12) in Sun et al. (2022), the LF $\Phi(L)$ is the sum of each event j in the range from $\log_{10} L$ to $\log_{10} L + d\log_{10} L$ (with a total of ΔN_L events):

$$\Phi(L) d\log_{10} L = \sum_{j=1}^{\Delta N_L} [\Phi(L) d\log_{10} L]_j = \sum_{j=1}^{\Delta N_L} \frac{1}{[T_{\rm BAT} \times V'_{\rm max}]_j}, \quad (1)$$

where $T_{\rm BAT}$ is the total monitoring time by Swift/Burst Alert Telescope (BAT) and $V'_{\rm max}$ is the effective maximum volume that is monitored (with the field of view $\Omega_{\rm BAT}$), weighted by the density evolution $f(z)$ and time dilation, i.e.,

$$V'_{\rm max} = \int_0^{z_{\rm max}} \frac{\Omega_{\rm BAT}}{4\pi} \cdot \frac{f(z)}{1+z} \frac{dV(z)}{dz} dz. \quad (2)$$

The $z_{\rm max}$ is the maximum redshift at which an event can be detected with bolometric peak luminosity $L_{\rm bol}$. The bolometric peak luminosities of these three events, defined in the energy range of 1–10^4 keV, are derived from k-correction based on the spectrum listed in Table 1, following Equation (29) in Sun et al. (2015).

We take the instrument parameters of Swift/BAT, with $\Omega_{\rm BAT} = 1.3$, $T_{\rm BAT} = 17$ yr, and flux sensitivity $f_{\rm th,BAT} = 3 \times 10^{-8}$ erg cm^{-2} s^{-1}. The $f(z)$ for GRBs with merger origins is adopted from Zhu et al. (2021b). We take the correction of the redshift measurement into account. For both the lGRB and sGRB samples, the ratio between the total number and the number of z-known events from the Swift observations is approximately 4: 1. In addition, since Swift has a relatively softer energy band than BATSE, it tends to detect more lGRBs than sGRBs. One needs to adopt another correction, by a factor of 3, to compensate for the short (hard)-to-long (soft) ratio of the Swift-detected GRBs in comparison with those from the BATSE observations (Sun et al. 2015).

We divide the events into two bins, with $\Delta \log_{10} L = 1$, and fit the LF with a single power law of the slope 0.6 ± 0.8. The local event-rate density, which is derived by integrating the LF above the luminosity threshold 3×10^{50} erg s^{-1}, is given as

$$\mathcal{R}_0(>3 \times 10^{50}\ {\rm erg\ s^{-1}}) = 2.4^{+2.3}_{-1.3} \times 10^{-2}\ {\rm Gpc^{-3}\ yr^{-1}}. \quad (3)$$

The errors are given at the 1σ confidence level (Gehrels 1986).

The intrinsic local event-rate densities of both lGRBs and sGRBs are of the order of unity, in the unit of Gpc^{-3} yr^{-1}, above the isotropically bolometric luminosity of $\sim 10^{50}$ erg s^{-1} (Sun et al. 2015). We find that the local event-rate density for lGRBs with merger origins is much lower than those for both lGRBs and sGRBs. The rate densities for BNSs inferred using GWs through GWTC-2 (GWTC-3) are 320^{+490}_{-240} Gpc^{-3} yr^{-1} (10–1700 Gpc^{-3} yr^{-1}) (e.g., Abbott et al. 2021b; the LIGO Scientific Collaboration et al. 2021; Mandel & Broekgaarden 2022). Abbott et al. (2021a) inferred an NSBH rate density of 45^{+75}_{-33} Gpc^{-3} yr^{-1}, by considering the observations of two NSBH mergers, or 130^{+112}_{-69} Gpc^{-3} yr^{-1}, assuming a broad NSBH population, while GWTC-3 (the LIGO Scientific Collaboration et al. 2021) reported the NSBH merger rate density as being between 7.8 and 140 Gpc^{-3} yr^{-1}. By considering a jet beaming factor of $f_{\rm b} = 0.01$, the beaming-corrected event-rate density for merger-origin lGRBs is $\mathcal{R}_{0,\rm b} = 2.4^{+2.3}_{-1.3} (f_{\rm b}/0.01)$ Gpc^{-3} yr^{-1}, which is much lower than those for BNS and NSBH mergers. However, the beaming-corrected rate density for merger-origin lGRBs is consistent with that for NS-first-born NSBH mergers ($\lesssim$20% of the total NSBH populations; Román-Garza et al. 2021; Chattopadhyay et al. 2022). By investigating the parameter space for forming NS-first-born NSBH binaries, Hu et al. (2022) found that most of the NSBH binaries that could merge within Hubble time would have BHs with projected aligned spins $\chi_{\rm BH} \gtrsim 0.8$, and, hence, could certainly make the tidal disruptions to produce EM counterparts. Only a small fraction of low-mass BHs with $\chi_{\rm BH} \sim 0.2$–0.8 could merge with an NS within Hubble time, and this could still allow tidal disruption to happen, if the NSs are not really massive (i.e., $M_{\rm NS} \gtrsim 1.6 - 2.0\, M_\odot$). Since the rest of the BH-first-born NSBH mergers would mostly contribute to plunging events, due to the negligible projected aligned spins of the BH components (Zhu et al. 2022), a single explosive population via an NS-first-born NSBH merger could account for their origin.

3. Modeling and Origin of GRB 211211A

GRB211211A, as a recent high-impact event, has one of the most complete multiband data records of afterglow and kilonova, which can give a strict constraint on our fitting parameters to explore its plausible origin. In this section, we will simultaneously interpret the emissions of gamma-ray/X-ray EEs via the fallback accretion of r-process heating materials, the afterglow emissions, and the kilonova emissions of GRB 211211A, within the framework of NSBH mergers. Since the structures of the prompt emissions of GRBs are generally believed to originate from internal shock processes, in the following discussion, we are only interested in the light-curve outline, which mainly depends on the engine power due to the fallback accretion.

3.1. Modeling

3.1.1. Fallback Accretion of r-process Heating Materials

For NSBH mergers with NS tidal disruption, a fraction of the r-process heating materials would fall back onto the remnant BH, tens of seconds after the merger, resulting in the EE (Metzger et al. 2010a; Desai et al. 2019), through the Blandford–Znajek (BZ) mechanism (Blandford & Znajek 1977). Following MacFadyen et al. (2001) and Dai & Liu (2012), the fallback rate initially increases with time, as $\dot{M} \propto t^{1/2}$, before the time of $t_{\rm p}$ corresponds to the peak fallback rate $\dot{M}_{\rm p}$. Then, the late-time fallback accretion behavior would track as $\dot{M} \propto t^{-5/3}$, until the break time $t_{\rm b}$ (Chevalier 1998). While most of the fallback materials are accreted after $t_{\rm b}$, we describe the fallback rate as $\dot{M} \propto t^{-s}$. An empirical three-segment broken power-law function is adopted to model the fallback accretion rate of the r-process heating materials, i.e.,

$$\dot{M}(t) = \dot{M}_{\rm p} \left[\frac{1}{2} \left(\frac{t - t_0}{t_{\rm p} - t_0} \right)^{-1/2} + \frac{1}{2} \left(\frac{t - t_0}{t_{\rm p} - t_0} \right)^{5/3} \right]^{-1} \times \left[1 + \frac{1}{2} \left(\frac{t - t_0}{t_{\rm b} - t_0} \right)^{s-5/3} \right]^{-1}, \quad (4)$$

where t_0 is the starting time of the fallback accretion.

The BZ power is related to the mass and spin of the central BH (e.g., Li & Paczyński 2000; Lei et al. 2013, 2017; Wu et al. 2013; Liu et al. 2017), i.e.,

$$L_{\rm BZ} = 1.7 \times 10^{50}\ {\rm erg\ s^{-1}} \chi_{\rm BH} \left(\frac{M_{\rm BH}}{M_\odot} \right)^2 B^2_{\rm BH,15} F(\chi_{\rm BH}), \quad (5)$$

where $M_{\rm BH}$ is the central BH mass, $\chi_{\rm BH}$ is the dimensionless aligned spin of the BH, $B_{\rm BH,15}=B_{\rm BH}/10^{15}$ G is the magnetic field strength threading the BH horizon, and $F(\chi_{\rm BH})=[(1+q^2)/q^2][(q+1/q)\arctan q-1]$ with $q=\chi_{\rm BH}/(1+\sqrt{1-\chi_{\rm BH}^2})$. The magnetic field can be estimated through the balance between the magnetic pressure on the horizon and the ram pressure of the innermost part of the accretion flow:

$$\frac{B_{\rm BH}^2}{8\pi}=P_{\rm ram}\sim\rho c^2\sim\frac{\dot{M}c}{4\pi r_{\rm H}^2}, \tag{6}$$

where c is the speed of light and $r_{\rm H}=(1+\sqrt{1-\chi_{\rm BH}^2})r_{\rm g}$ is the radius of the BH horizon, with the Schwarzschild radius $r_{\rm g}=GM_{\rm BH}/c^2$ and the gravitational constant G. Thus, the BZ power can be also expressed as

$$L_{\rm BZ}=9.3\times10^{53}\,{\rm erg\,s^{-1}}\times\frac{\chi_{\rm BH}^2F(\chi_{\rm BH})}{(1+\sqrt{1-\chi_{\rm BH}^2})^2}\frac{\dot{M}}{M_\odot\,{\rm s^{-1}}}. \tag{7}$$

Because the central BH would be spun up by accretion and spun down by the BZ mechanism, the conservation of the energy and angular momentum of a BH can be written as

$$\frac{dM_{\rm BH}c^2}{dt}=\dot{M}c^2E_{\rm ISCO}-L_{\rm BZ},$$
$$\frac{dJ_{\rm BH}}{dt}=\dot{M}J_{\rm ISCO}-2L_{\rm BZ}/\Omega_{\rm H}, \tag{8}$$

where $\Omega_{\rm H}=c\chi_{\rm BH}/(2r_{\rm H})$ is the angular velocity of the BH horizon and $E_{\rm ISCO}=(4\sqrt{\widetilde{R}_{\rm ISCO}}-3\chi_{\rm BH})/\sqrt{3}\widetilde{R}_{\rm ISCO}$ and $J_{\rm ISCO}=2GM_{\rm BH}(3\sqrt{\widetilde{R}_{\rm ISCO}}-2\chi_{\rm BH})/c\sqrt{3\widetilde{R}_{\rm ISCO}}$ are the specific energy and specific angular momentum of a particle at the innermost stable circular orbit (ISCO) radius (Novikov & Thorne 1973), respectively. $\widetilde{R}_{\rm ISCO}=3+Z_2-{\rm sign}(\chi_{\rm BH})\sqrt{(3-Z_1)(3+Z_1+2Z_2)}$ represents the normalized radius of the BH ISCO with $Z_1=1+(1-\chi_{\rm BH}^2)^{1/3}[(1+\chi_{\rm BH})^{1/3}+(1-\chi_{\rm BH})^{1/3}]$ and $Z_2=\sqrt{3\chi_{\rm BH}^2+Z_1^2}$ (Bardeen et al. 1972). Since the angular momentum of BH is expressed as $J_{\rm BH}=GM_{\rm BH}^2\chi_{\rm BH}/c$, one has

$$\frac{d\chi_{\rm BH}}{dt}=\frac{(\dot{M}J_{\rm ISCO}-2L_{\rm BZ}/\Omega_{\rm H})c}{GM_{\rm BH}^2}-\frac{2\chi_{\rm BH}(\dot{M}c^2E_{\rm ISCO}-L_{\rm BZ})}{M_{\rm BH}c^2}. \tag{9}$$

By combing Equations (7), (8), and (9), the time-evolving BZ power can thus be calculated. The observed gamma-ray/X-ray light curve caused by the fallback accretion is connected to the BZ power via the gamma-ray/X-ray radiation efficiency $\eta_{(\gamma,{\rm X})}$ and the jet beaming factor $f_{\rm b}$, i.e.,

$$\eta_{(\gamma,{\rm X})}L_{\rm BZ}=f_{\rm b}L_{(\gamma,{\rm X})}. \tag{10}$$

3.1.2. Jet Afterglow Emissions

In order to calculate the afterglow light curves, we adopt the Gaussian structured jet model (e.g., Zhang & Mészáros 2002), which was favored by the observations of the GRB 170817A afterglow (e.g., Lamb & Kobayashi 2018; Lazzati et al. 2018; Mooley et al. 2018; Troja et al. 2018; Xie et al. 2018), i.e.,

$$E(\theta)=E_0\exp\left(-\frac{\theta^2}{2\theta_{\rm c}^2}\right), \tag{11}$$

where E_0 is the on-axis equivalent isotropic energy and $\theta_{\rm c}$ is the characteristic core angle. The spectra of the standard synchrotron emissions from relativistic electrons are employed following Sari et al. (1998), Kumar & Zhang (2015), and Zhang (2018). For more details of the afterglow modeling that we apply to calculate the sGRB light curves along the line of sight, see Appendix C in Zhu et al. (2021b). We constrain the afterglow parameters, including E_0, $\theta_{\rm c}$, the viewing angle $\theta_{\rm v}$ with respect to the moving direction of the jet, the circumburst number density n, the power-law index of the electron distribution p, and the fraction of the shock energy carried by the magnetic fields ε_B, to fit the multiband light curves of GRB 211211A. The fraction of the shock energy carried by electrons is set to its typical value of $\varepsilon_e=0.1$.

3.1.3. Ejecta Mass

After NSBH mergers, a fraction of the neutron-rich matter (i.e., an unbound dynamical ejecta) is tidally ejected, while an accretion disk is formed around the remnant BH. The total remnant mass outside the remnant and the dynamical ejecta mass is dependent on the NSBH system parameters, including the BH mass $M_{\rm BH}$, the dimensionless spin parameter projected onto the orientation of the orbital angular momentum $\chi_{\rm BH}$, the NS mass $M_{\rm NS}$, and the NS equation of state (EoS), which can be calculated based on an empirical fitting formula, i.e.,

$$\frac{M_{\rm fit}}{M_{\rm NS}^{\rm b}}=\left[\max\left(a_1\frac{1-2C_{\rm NS}}{\eta^{1/3}}-a_2\widetilde{R}_{\rm ISCO}\frac{C_{\rm NS}}{\eta}+a_3,0\right)\right]^{a_4}, \tag{12}$$

where $M_{\rm NS}^{\rm b}$ is the baryonic mass of the NS, $C_{\rm NS}$ is the compactness of the NS determined by the NS EoS, $\eta=Q/(1+Q)^2$, and $Q=M_{\rm BH}/M_{\rm NS}$ is the mass ratio between the primary BH mass and the secondary NS mass. For the fitting formula of the total remnant mass $M_{\rm tot,fit}$ (the dynamical ejecta mass $M_{\rm d,fit}$), the parameters in Equation (12) are $a_1=0.406$, $a_2=0.139$, $a_3=0.255$, and $a_4=1.761$ ($a_1=0.218$, $a_2=0.028$, $a_3=-0.122$, and $a_4=1.358$), obtained from Foucart et al. (2018) (Zhu et al. 2020). Since the fitting formulas of the total remnant mass and the dynamical ejecta mass are obtained with independent simulation data, one needs to set an upper limit on the maximum fraction of dynamical ejecta mass to total remnant mass, i.e., $M_{\rm d,max}\approx f_{\rm max}M_{\rm total,fit}$. We set $f_{\rm max}\approx0.5$, based on the simulation results from Kyutoku et al. (2015). Therefore, the final empirical mass of the dynamical ejecta is $M_{\rm d}\approx\min(M_{\rm d,fit},f_{\rm max}M_{\rm total,fit})$.

We consider two ejecta components for NSBH kilonova model, i.e., the wind ejecta from the disk around the remnant BH and the dynamical ejecta caused by tidal forces. The wind ejecta mass can be estimated as a constant fraction of the disk mass, i.e., $M_{\rm w}\approx\xi_{\rm w}M_{\rm disk}$, where $\xi_{\rm w}\approx0.2$ (Fernández et al. 2015; Just et al. 2015; Siegel & Metzger 2017).

Numerical simulations have revealed that the dynamical ejecta from NSBH mergers are highly anisotropic and distributed in the equatorial plane (Kyutoku et al. 2015; Kawaguchi et al. 2016;

Darbha et al. 2021). Zhu et al. (2020) constructed a viewing angle–dependent model for NSBH kilonovae, and found that the wind ejecta can be covered by the dynamical ejecta for a large $\theta_{\rm v}$ condition. However, for the case of GRB 211211A, observed from the on-axis or near-on-axis view (i.e., $\theta_{\rm v}\sim 0^{\circ}$), one can simultaneously see two components. Hereafter, in order to reduce the computational complexity, we use a simplified model based on Zhu et al. (2020), to separately consider the emissions from the wind ejecta and the dynamical ejecta.

Assuming that the wind ejecta has an isotropic density profile and a homologous expansion, we adopt the common analytic solution derived by Arnett (1982) and Chatzopoulos et al. (2012) for calculating the bolometric luminosity of the wind ejecta:

$$L_{\rm w}(t)=e^{-(t'/t_{\rm w,diff})^2}\int_0^t 2L_{\rm w,in}(t')\frac{t'}{t_{\rm w,diff}}e^{(t'/t_{\rm w,diff})^2}\frac{dt'}{t_{\rm w,diff}}, \quad (13)$$

where $t_{\rm w,diff}=(2\kappa_{\rm w}M_{\rm w}/\beta v_{\rm w}c)^{1/2}$ is the photon diffusion timescale of the wind ejecta, $\kappa_{\rm w}$ is the gray opacity, and $\beta=13.8$ is the dimensionless constant. $L_{\rm w,in}(t)=\epsilon_{Y_e}\epsilon_{\rm th}\dot{\epsilon}(t)M_{\rm w}$ represents the injection heating rate from the radioactive decay of the r-process nucleus, where $\epsilon_{Y_e}=0.5+2.5[1+e^{4(t/{\rm day}-1)}]^{-1}$, if $Y_e\leqslant 0.25$ ($\epsilon_{Y_e}=1$ otherwise) is an electron fraction–dependent term that takes into account extremely neutron-rich ejecta with a decay half-life of a few hours (Perego et al. 2017), $\epsilon_{\rm th}\approx 0.5$ is the efficiency of thermalization (Metzger et al. 2010b), and $\dot{\epsilon}(t)=\dot{\epsilon}_0(t/{\rm day})^{-\alpha}$ is the specific energy injection rate due to radioactive decay, with $\dot{\epsilon}_0\approx 1.58\times 10^{10}$ erg g^{-1} s^{-1} and $\alpha\approx 1.3$ (Korobkin et al. 2012).

In order to calculate the monochromatic light curves of the wind ejecta, we define a photosphere temperature as

$$T_{\rm w,phot}(t)=\max\left[\left(\frac{L_{\rm w}(t)}{4\pi\sigma_{\rm SB}v_{\rm w}^2t^2}\right)^{1/4},T_{\rm La}\right], \quad (14)$$

where $\sigma_{\rm SB}$ is the Stefan–Boltzmann constant, $v_{\rm w}\approx 0.067\,c$ is assumed to be the wind ejecta velocity (e.g., Just et al. 2015; Perego et al. 2017; Siegel & Metzger 2017), and $T_{\rm La}\approx 1000$ K is the first ionization temperature of lanthanides (Barnes & Kasen 2013). The photosphere radius can be written as

$$R_{\rm w,phot}(t)=\begin{cases}v_{\rm w}t, & \text{for } T_{\rm w,phot}>T_{\rm La},\\ \left(\dfrac{L_{\rm w}(t)}{4\pi\sigma_{\rm SB}T_{\rm La}^4}\right)^{1/2}, & \text{for } T_{\rm w,phot}=T_{\rm La},\end{cases} \quad (15)$$

then the flux density contributed from the emission of the wind ejecta is given by

$$F_{\nu,{\rm w}}=\frac{8\pi^2R_{\rm w,phot}^2}{h^2c^2}\frac{h^3\nu^3}{\exp(h\nu/k_{\rm B}T_{\rm w,phot}-1)}\frac{1}{4\pi D_{\rm L}^2}, \quad (16)$$

where h, $k_{\rm B}$, and ν represent the Planck constant and the Boltzmann constant and frequency, respectively.

Based on the simulations of NSBH mergers (Kyutoku et al. 2015), the mass distribution of the dynamical ejecta is highly anisotropic, with the mass mainly distributed around the equatorial plane and shaped like a crescent. The dynamical ejecta is typically concentrated around the orbital plane, with a half-opening angle in the latitudinal direction of $\theta_{\rm d}\approx 15^{\circ}$, and often sweeps out only a half of the plane, i.e., an opening angle in the longitudinal direction of $\varphi_{\rm d}\approx 180^{\circ}$. Since the dynamical ejecta is geometrically thin in the latitudinal direction, the photons would always be diffused from the latitudinal edge. Due to the $dM_{\rm d}/dv\approx$ const between the radial velocity range of $v_{\rm d,min}<v<v_{\rm d,max}$, based on the numerical relativity simulations (Kyutoku et al. 2015), the bolometric luminosity of the dynamical ejecta can be obtained from Kawaguchi et al. (2016), i.e.,

$$L_{\rm d}(t)\approx(1+\theta_{\rm d})\epsilon_{\rm th}\dot{\epsilon}_0M_{\rm d}\times\begin{cases}\dfrac{t}{t_{\rm c}}\left(\dfrac{t}{\rm day}\right)^{-\alpha}, & \text{for } t<t_{\rm c},\\ \left(\dfrac{t}{\rm day}\right)^{-\alpha}, & \text{for } t>t_{\rm c},\end{cases} \quad (17)$$

where $t_{\rm c}=[\kappa_{\rm d}\theta_{\rm d}M_{\rm d}/2c\varphi_{\rm d}(v_{\rm d,max}-v_{\rm d,min})]^{1/2}$ is defined as the critical diffuse timescale on which all ejecta can be seen. We set the minimum velocity $v_{\rm d,min}\approx 0.1\,c$, following the simulations of Kyutoku et al. (2015), while the maximum velocity can be estimated as $v_{\rm d,max}=\sqrt{3v_{\rm d,rms}^2-3v_{\rm d,min}^2/4}-v_{\rm d,min}/2$, where $v_{\rm d,rms}=(-0.441Q^{-0.224}+0.539)c$ is the root-mean-square velocity of the dynamical ejecta obtained from Zhu et al. (2020).

Because $dL_{\rm d}/2$ is released over an area of $\varphi_{\rm d}vt^2dv$, one can derive the photosphere temperature of each velocity at a given time:

$$T_{\rm d,phot}(v,t)\approx\left[\frac{L_{\rm d}(t)}{2\sigma_{\rm SB}\varphi_{\rm d}v(v_{\rm d,max}-v_{\rm d,min})t^2}\right]^{1/4}. \quad (18)$$

Table 2
Priors and Results for the Fitting Parameters

Parameter	Prior	Min	Max	Result
$M_{\rm BH}/M_{\odot}$	Flat	2.22	15	$8.21^{+0.77}_{-0.75}$
$\chi_{\rm BH}$	Flat	0	0.997	$0.62^{+0.06}_{-0.07}$
$M_{\rm NS}/M_{\odot}$	Gaussian	1.0	2.22	$1.23^{+0.06}_{-0.07}$
$\kappa_{\rm w}$/cm^2 g^{-1}	Flat	0.5	5	$0.56^{+0.13}_{-0.05}$
$\kappa_{\rm d}$/cm^2 g^{-1}	Flat	10	100	$11.0^{+1.4}_{-0.8}$
$\dot{M}_{\rm p}/M_{\odot}$ s^{-1}	Log-flat	10^{-10}	1	$2.19^{+0.44}_{-0.37}\times 10^{-5}$
t_0/s	Log-flat	10	12.7	$11.2^{+0.0}_{-0.0}$
$t_{\rm p}$/s	Log-flat	12.7	40	$30.2^{+0.0}_{-0.0}$
$t_{\rm b}$/s	Log-flat	100	1000	234^{+0}_{-0}
s	Flat	0	15	$7.33^{+0.19}_{-0.19}$
η_{γ}	Log-flat	10^{-2}	1	$0.29^{+0.00}_{-0.00}$
E_0/erg	Log-flat	10^{50}	10^{53}	$5.1^{+2.6}_{-1.9}\times 10^{52}$
$\theta_{\rm c}$/rad	Flat	0	0.2	$0.03^{+0.00}_{-0.00}$
$\theta_{\rm v}$/rad	Flat	0	0.5	$0.07^{+0.01}_{-0.01}$
p	Flat	2	3	$2.01^{+0.01}_{-0.01}$
n/g cm^{-3}	Log-flat	10^{-6}	2	$0.41^{+0.77}_{-0.30}$
ϵ_B	Log-flat	10^{-5}	1	$1.3^{+1.8}_{-0.6}\times 10^{-3}$

Note. The prior of $M_{\rm NS}$ is adopted as a Gaussian distribution, i.e., $\mathcal{N}(M_{\rm NS}/M_{\odot})\sim(\mu=1.3,\sigma=0.11)$, consistent with the observed mass distributions of NSs in Galactic BNS systems (Lattimer 2012).

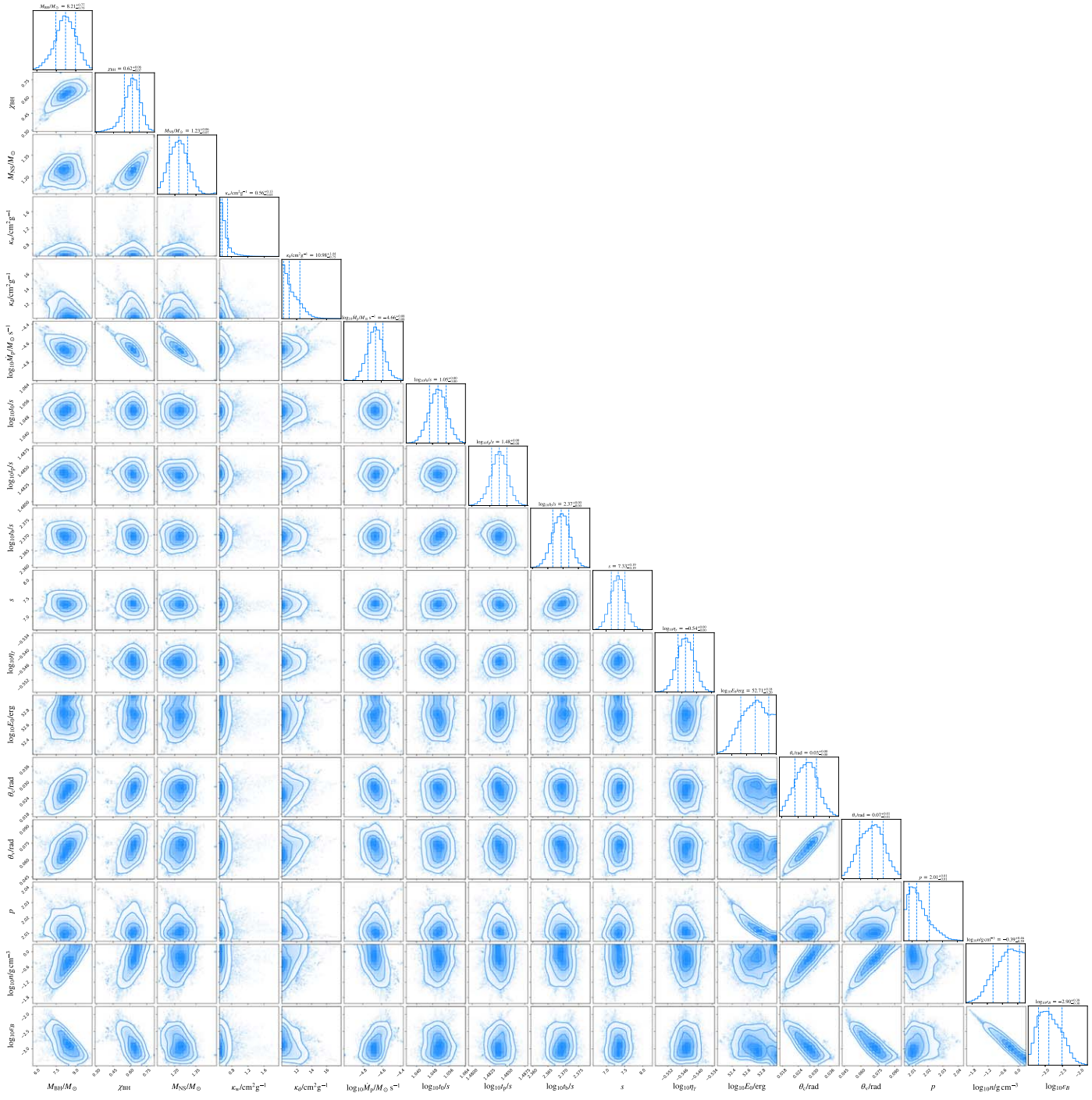

Figure 4. The posteriors of the fitting parameters. The medians and 1σ credible intervals are labeled.

The total flux density from the dynamical ejecta can be expressed as

$$F_{\nu,\rm d} \approx \int_{\nu_{\rm d,min}}^{\nu_{\rm d,max}} \frac{4\pi\varphi_{\rm d}\nu t^2}{h^2c^2}\frac{h^3\nu^3}{\exp(h\nu/k_{\rm B}T_{\rm d,phot}-1)}\frac{1}{4\pi D_{\rm L}^2}d\nu. \quad (19)$$

3.2. Origins of GRB 211211A and Associated Kilonova

For simplicity, we directly use the final BH mass $M_{\rm BH,f}$ and the final dimensional aligned spin $\chi_{\rm BH,f}$ after NSBH mergers, based on Equation (3) and Equation (5) from Deng (2020), as functions of the initial NSBH system parameters, i.e., $M_{\rm BH}$, $M_{\rm NS}$, $C_{\rm NS}$, and $\chi_{\rm BH}$, to determine the BZ power. The observed mass distributions of Galactic BNS systems (Lattimer 2012) were inferred to be Gaussian distributions, i.e., $\mathcal{N}(M_{\rm NS}/M_\odot) \sim (\mu = 1.3, \sigma = 0.11)$. The observations of GW200105 and GW200115 showed that their NS masses are $\sim$1.9 $M_\odot$ and $\sim$1.5 $M_\odot$ (Abbott et al. 2021a), plausibly more massive than the mass distributions of Galactic BNS systems. Furthermore, some population synthesis simulations have predicted that NSBH mergers may usually contain more massive NSs compared to those in BNS mergers (e.g., Giacobbo & Mapelli 2018; Broekgaarden et al. 2021).

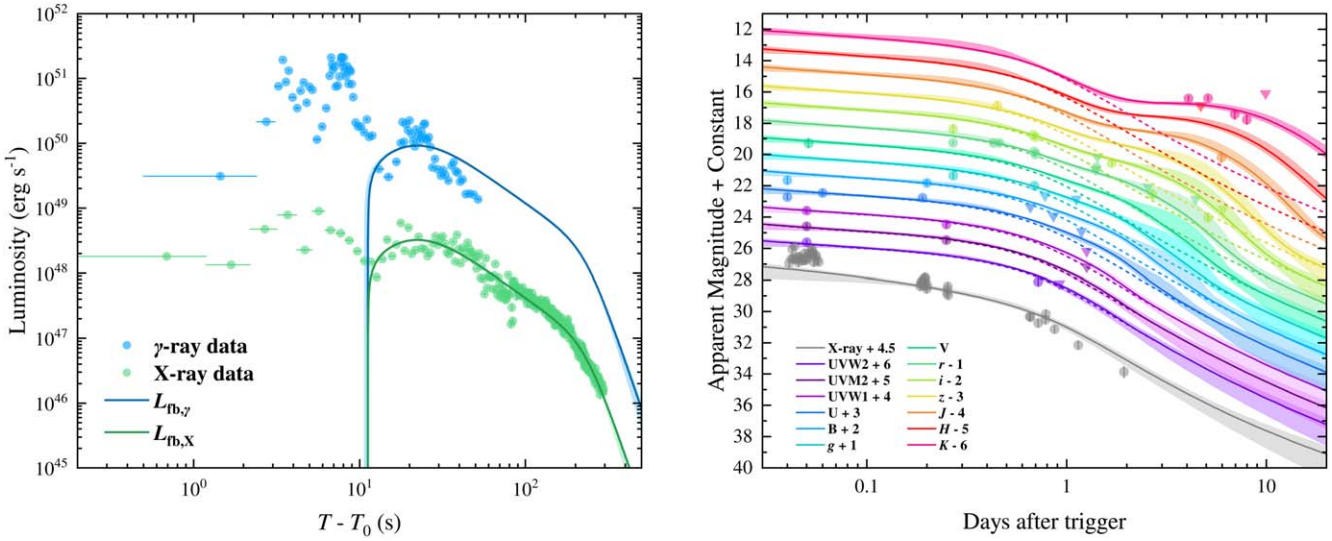

Figure 5. Left: Gamma-ray (blue points from Yang et al. 2022) and X-ray (green points from BAT and XRT) light curves of GRB 211211A. The blue and green lines are the fittings of the EEs using the fallback accretion model. Right: the detections (circles) and upper limits (inverted triangles) of the multiband data for the GRB 211211A afterglow and associated kilonova emissions. The solid lines and shaded areas represent the best fits and 90% credible intervals for the multiband data, while the contributions from the afterglow emissions are marked as the dashed lines.

However, due to the currently limited observations of NSBH GWs, which could hardly represent a complete mass distribution of the NSs in NSBH mergers, we use the observed mass distribution of the NSs in Galactic BNS systems as the prior of the NS mass. Here, an EoS of AP4 (Akmal & Pandharipande 1997) is adopted, since it is one of the most likely EoSs constrained by GW170817 (Abbott et al. 2018). In our calculations, we set $\eta_{\rm X} = 0.01$ and $f_{\rm b} = 0.01$, while η_γ is assumed to be a fitting parameter.

In theory, NSBH kilonovae were thought to be optically dim, but infrared-bright, compared with BNS kilonovae (e.g., Kasen et al. 2017; Kawaguchi et al. 2020; Zhu et al. 2020), because an NSBH merger probably produces a large number of lanthanide-rich dynamical ejecta with opacity $\kappa_{\rm d} \sim 10$–$100\ {\rm cm^2\ g^{-1}}$. The disk wind ejecta is hardly likely to be lanthanide-poor, due to the lack of shock heating and neutrino irradiation during or shortly after the merger (e.g., Fernández et al. 2015; Just et al. 2015). However, Fujibayashi et al. (2020) and Kyutoku et al. (2020) recently found that the wind ejecta can still be lanthanide-poor if the viscous coefficient is not extremely high. Given the uncertainty of the wind ejecta, we adopt a wide prior distribution for the wind ejecta opacity, which is $\kappa_{\rm w} \sim 0.5$–$5\ {\rm cm^2\ g^{-1}}$.

There are 17 free parameters, summarized in Table 2. The Markov Chain Monte Carlo method with the `emcee` package (Foreman-Mackey et al. 2013) is adopted to simultaneously fit the data of the gamma-ray/X-ray EEs, afterglow, and kilonova emissions of GRB 211211A. We summarize the 17 free parameters and their fitting results with 1σ credible intervals in Table 2, while the posteriors of these fitting parameters are shown in Figure 4. Except for $\kappa_{\rm w}$ and $\kappa_{\rm d}$, these fitting parameters are convergent. The lower value of $\kappa_{\rm w}$ indicates that the wind ejecta of NSBH mergers could be lanthanide-poor. The best-fit light curves of the gamma-ray/X-ray EEs, afterglow, and kilonova emissions are shown in Figure 5.

Our fitting results reveal that GRB 211211A could be a merger between a $\sim 1.23^{+0.06}_{-0.07}\ M_\odot$ NS and a $\sim 8.21^{+0.77}_{-0.75}\ M_\odot$ BH, with an aligned spin of $\chi_{\rm BH} \sim 0.62^{+0.06}_{-0.07}$. The merger would produce ~ 0.005–$0.03\ M_\odot$ lanthanide-poor wind ejecta and ~ 0.015–$0.025\ M_\odot$ lanthanide-rich dynamical ejecta. In Section 2.2, we suspected that GRB 211211A could have originated from an NS-first-born NSBH merger, based on the estimations of the event-rate density. Hu et al. (2022) found that for an NS-first-born NSBH binary system, the companion helium star would be efficiently tidally spun up by the NS, and would thus finally form a fast-spinning BH whose aligned spin would always be $\chi_{\rm BH} \gtrsim 0.8$. Thus, the mass and spin of the BH component for GRB 211211A are essentially consistent with those of NS-first-born NSBH mergers, as predicted by Hu et al. (2022).

Our fitting results show that the fallback accretion for the interpretation of the EE starts at $t_0 = 11.2$ s, peaks at $t_{\rm p} = 30.2$ s, and breaks at around $t_{\rm b} = 234$ s in the rest frame. The peak fallback accretion rate is $\dot{M}_{\rm p} \sim 2 \times 10^{-5}\ M_\odot\ {\rm s^{-1}}$. Using Equation (4), one can estimate the fallback mass as $M_{\rm fb} \simeq \int_{t_0}^{t_{\rm b}} \dot{M} dt \approx 1 \times 10^{-3}\ M_\odot$. The start time and peak accretion rate are consistent with the predictions of Desai et al. (2019). Furthermore, Desai et al. (2019) predicted that rebrightening EEs, caused by the fallback accretion of r-process heating materials, may only occur if the remnant BH has a mass of $\gtrsim 6$–$8\ M_\odot$. Based on the fitting results, GRB 211211A would finally form a $\sim 10 M_\odot$ BH after the NSBH merger, so our interpretations for the origin of GRB 211211A are self-consistent.

There are some uncertainties in our fitting results. Our results reveal that the mass ratio between the BH and the NS is ~ 7 for GRB 211211A. Due to the presently limited simulations for NS-first-born NSBH mergers, it is not known if NSBH systems with such high mass ratios are common in the universe. More detailed simulations of the populations of NS-first-born NSBH mergers, based on population synthesis and detailed binary evolution, are suggested for the future. We also find that a ~ 0.005–$0.03\ M_\odot$ lanthanide-poor wind ejecta is needed in order to explain the observations of the kilonova emission associated with GRB 211211A. A large amount of lanthanide-poor wind ejecta are not typically expected to be produced after NSBH mergers (e.g., Fernández et al. 2015; Just et al. 2015),

although Fujibayashi et al. (2020) and Kyutoku et al. (2020) have found that NSBH mergers can still lead to considerable lanthanide-poor wind ejecta, if the viscous coefficient is not extremely high. Future multimessenger observations between NSBH GWs and their associated kilonova emissions will help us to constrain the mass fraction of *r*-process elements for the wind ejecta from NSBH mergers.

4. Discussions and Conclusion

In this *Letter*, we collect three unique merger-origin bursts, i.e., GRB 060614, GRB 211211, and GRB 211227A, to study their observed properties and explore their possible origins. Both the MEs and EEs of these bursts are long-duration, which fall into the distribution of lGRB populations. When the redshift information is considered, we find that the WEs of these three bursts still behave as normal lGRBs, but that their MEs lie on the sGRB track of the Amati relation. These similar observed properties are characterized differently than those of classical collapsar-origin lGRBs and merger-origin sGRBs with/without EEs, indicating a unique origin for these three bursts. Their X-ray MEs and EEs show unambiguous fallback accretion signatures, decreasing as $\propto t^{-5/3}$, which extend the burst durations. The EEs might result from the fallback of *r*-process heating materials, which is predicted to occur after NSBH mergers. The beaming-corrected local event-rate density of these merger-origin lGRBs is estimated to be $\mathcal{R}_{0,\rm b} \sim 2.4^{+2.3}_{-1.3}(f_{\rm b}/0.01)\,{\rm Gpc^{-3}yr^{-1}}$. This local event-rate density is much lower than that for BNS and NSBH mergers in the universe, but is consistent with the local event-rate density of NS-first-born mergers.

Our detailed analysis of the EE, using the fallback accretion model, afterglow, and kilonova of the recent high-impact event GRB 211211A, reveals that it could be a merger between a $\sim 1.23^{+0.06}_{-0.07}\,M_\odot$ NS and a $\sim 8.21^{+0.77}_{-0.75}\,M_\odot$ BH, with a dimensionless aligned spin parameter of $\chi_{\rm BH} \sim 0.62^{+0.06}_{-0.07}$, supporting an NS-first-born NSBH formation channel. We find that the fallback accretion for the interpretation of the EE starts at $t_0 = 11.2$ s and peaks at $t_{\rm p} = 30.2$ s, with a peak accretion rate of $\dot{M}_{\rm p} \sim 2 \times 10^{-5}\,M_\odot\,{\rm s^{-1}}$. The fallback mass is $M_{\rm fb} \sim 1 \times 10^{-3}\,M_\odot$. The start time and the peak accretion rate are consistent with the fallback accretion of *r*-process heating materials predicted by Desai et al. (2019). After the completion of this Letter, we notice that Y. Z. Meng et al. (2022, in preparation) have also showed that GRB 211211A could originate from an NSBH system in the photosphere emission model, whose long duration is from the duration-stretching effect of the saturated photosphere. Furthermore, Yang et al. (2015) have reported that the kilonova candidate associated with GRB 060614 had an ejection of $\sim 0.1\,M_\odot$ of *r*-process material. Yang et al. (2015) suggested that such significant ejected mass, within the possible range of dynamical ejecta of mergers between NSs and BHs with extreme high aligned spins (e.g., Lovelace et al. 2013; Kyutoku et al. 2015), strongly favored its origin being an NSBH merger rather than a BNS merger. Since NS-first-born NSBH mergers can easily cause tidal disruption, while the rest of BH-first-born NSBH mergers mostly contribute to plunging events, NSBH mergers can well interpret the origins of these GRBs. A long-duration burst, with a rebrightening fallback accretion signature of *r*-process heating materials after the ME, and a bright kilonova emission, might be commonly observed features for on-axis NSBH mergers.

Based on the estimated local event-rate of merger-origin lGRBs, if they certainly originate from NS-first-born NSBH mergers, the GW detection rates of NSBH mergers with fast-spinning primary BHs in the GW fourth observing run (O4) and fifth observing run (O5) of the LIGO/Virgo/KAGRA Collaboration are $\sim 10\,{\rm yr^{-1}}$ and $\sim 100\,{\rm yr^{-1}}$ (Zhu et al. 2021b), respectively. By assuming that all of the associated kilonova emissions can be detected, we estimate the multimessenger detection rates between GWs, GRBs, and kilonova emissions from NSBH mergers in O4 and O5 to be $\sim 0.1(f_{\rm b}/0.01)\,{\rm yr^{-1}}$ and $\sim 1(f_{\rm b}/0.01){\rm yr^{-1}}$, respectively. Thus, the smoking gun evidence for the NSBH merger origin of lGRBs and kilonovae will likely be verified in O5.

The authors acknowledge an anonymous referee for useful discussions. We also thank Jun Yang, Bing Zhang, Bin-Bin Zhang, He Gao, Shun-Ke Ai, and Yun-Wei Yu for helpful comments. This work is supported by the National Natural Science Foundation of China (grant Nos. 11773003, 11833003, 12003028, 12103065, 12121003, 12133003, 12192220, 12192221, U1931201, and U2038105), the National Basic Research Program of China (grant No. 2014CB845800), the China Manned Spaced Project (CMS-CSST-2021-B11), the Natural Science Foundation of Universities in Anhui Province (grant No. KJ2021A0106), and the National Key Research and Development Programs of China (2018YFA0404204).

Software: `Python`, https://www.python.org; `HEASoft` (Nasa High Energy Astrophysics Science Archive Research Center (Heasarc), 2014), http://heasarc.gsfc.nasa.gov/ftools; `scikit-learn`, https://scikit-learn.org/stable/index.html; `emcee` (Foreman-Mackey et al. 2013); `corner` (Foreman-Mackey 2016).

ORCID iDs

Jin-Ping Zhu https://orcid.org/0000-0002-9195-4904
Xiangyu Ivy Wang https://orcid.org/0000-0002-9738-1238
Hui Sun https://orcid.org/0000-0002-9615-1481
Yuan-Pei Yang https://orcid.org/0000-0001-6374-8313
Rui-Chong Hu https://orcid.org/0000-0002-6442-7850
Ying Qin https://orcid.org/0000-0002-2956-8367
Shichao Wu https://orcid.org/0000-0002-9188-5435

References

Abbott, B. P., Abbott, R., Abbott, T. D., et al. 2017a, PhRvL, 119, 161101
Abbott, B. P., Abbott, R., Abbott, T. D., et al. 2017b, ApJL, 848, L13
Abbott, B. P., Abbott, R., Abbott, T. D., et al. 2017c, ApJL, 848, L12
Abbott, B. P., Abbott, R., Abbott, T. D., et al. 2018, PhRvL, 121, 161101
Abbott, R., Abbott, T. D., Abraham, S., et al. 2021a, ApJL, 915, L5
Abbott, R., Abbott, T. D., Abraham, S., et al. 2021b, ApJL, 913, L7
Akmal, A., & Pandharipande, V. R. 1997, PhRvC, 56, 2261
Amati, L., Frontera, F., Tavani, M., et al. 2002, A&A, 390, 81
Anand, S., Coughlin, M. W., Kasliwal, M. M., et al. 2021, NatAs, 5, 46
Andreoni, I., Kool, E. C., Sagués Carracedo, A., et al. 2020, ApJ, 904, 155
Arcavi, I., Hosseinzadeh, G., Howell, D. A., et al. 2017, Natur, 551, 64
Arnett, W. D. 1982, ApJ, 253, 785
Bardeen, J. M., Press, W. H., & Teukolsky, S. A. 1972, ApJ, 178, 347
Barnes, J., & Kasen, D. 2013, ApJ, 775, 18
Belczynski, K., Klencki, J., Fields, C. E., et al. 2020, A&A, 636, A104
Berger, E. 2007, ApJ, 670, 1254
Blandford, R. D., & Znajek, R. L. 1977, MNRAS, 179, 433
Bloom, J. S., Kulkarni, S. R., Harrison, F., et al. 1998, ApJL, 506, L105
Bloom, J. S., Sigurdsson, S., & Pols, O. R. 1999, MNRAS, 305, 763
Broekgaarden, F. S., & Berger, E. 2021, ApJL, 920, L13
Broekgaarden, F. S., Berger, E., Neijssel, C. J., et al. 2021, MNRAS, 508, 5028
Chang, X.-Z., Lü, H.-J., Chen, J.-M., & Liang, E.-W. 2022, arXiv:2206.11438

Chattopadhyay, D., Stevenson, S., Broekgaarden, F., Antonini, F., & Belczynski, K. 2022, MNRAS, 513, 5780
Chattopadhyay, D., Stevenson, S., Hurley, J. R., Bailes, M., & Broekgaarden, F. 2021, MNRAS, 504, 3682
Chatzopoulos, E., Wheeler, J. C., & Vinko, J. 2012, ApJ, 746, 121
Chevalier, R. A. 1998, ApJ, 499, 810
Christensen, L., Hjorth, J., & Gorosabel, J. 2004, A&A, 425, 913
Coughlin, M. W., Dietrich, T., Antier, S., et al. 2020, MNRAS, 497, 1181
Coulter, D. A., Foley, R. J., Kilpatrick, C. D., et al. 2017, Sci, 358, 1556
Dai, Z. G., & Liu, R.-Y. 2012, ApJ, 759, 58
Darbha, S., Kasen, D., Foucart, F., & Price, D. J. 2021, ApJ, 915, 69
D'Avanzo, P., Malesani, D., Covino, S., et al. 2009, A&A, 498, 711
Della Valle, M., Chincarini, G., Panagia, N., et al. 2006, Natur, 444, 1050
Deng, C.-M. 2020, MNRAS, 497, 643
Desai, D., Metzger, B. D., & Foucart, F. 2019, MNRAS, 485, 4404
Di Clemente, F., Drago, A., & Pagliara, G. 2022, ApJ, 929, 44
D'Orazio, D. J., Haiman, Z., Levin, J., Samsing, J., & Vigna-Gómez, A. 2022, ApJ, 927, 56
Drout, M. R., Piro, A. L., Shappee, B. J., et al. 2017, Sci, 358, 1570
Drozda, P., Belczynski, K., O'Shaughnessy, R., Bulik, T., & Fryer, C. L. 2020, arXiv:2009.06655
Eichler, D., Livio, M., Piran, T., & Schramm, D. N. 1989, Natur, 340, 126
Evans, P. A., Cenko, S. B., Kennea, J. A., et al. 2017, Sci, 358, 1565
Fernández, R., Foucart, F., Kasen, D., et al. 2017, CQGra, 34, 154001
Fernández, R., Kasen, D., Metzger, B. D., & Quataert, E. 2015, MNRAS, 446, 750
Fong, W., Berger, E., & Fox, D. B. 2010, ApJ, 708, 9
Fong, W., Berger, E., Margutti, R., & Zauderer, B. A. 2015, ApJ, 815, 102
Foreman-Mackey, D. 2016, JOSS, 1, 24
Foreman-Mackey, D., Hogg, D. W., Lang, D., & Goodman, J. 2013, PASP, 125, 306
Foucart, F., Hinderer, T., & Nissanke, S. 2018, PhRvD, 98, 081501
Fragione, G. 2021, ApJL, 923, L2
Fujibayashi, S., Shibata, M., Wanajo, S., et al. 2020, PhRvD, 101, 083029
Gal-Yam, A., Fox, D. B., Price, P. A., et al. 2006, Natur, 444, 1053
Galama, T. J., Vreeswijk, P. M., van Paradijs, J., et al. 1998, Natur, 395, 670
Gao, H., Lei, W.-H., & Zhu, Z.-P. 2022, ApJL, 934, L12
Gehrels, N. 1986, ApJ, 303, 336
Ghirlanda, G., Salafia, O. S., Paragi, Z., et al. 2019, Sci, 363, 968
Giacobbo, N., & Mapelli, M. 2018, MNRAS, 480, 2011
Goldstein, A., Veres, P., Burns, E., et al. 2017, ApJL, 848, L14
Goldstein, A., Hamburg, R., Wood, J., et al. 2019, arXiv:1903.12597
Gompertz, B. P., Levan, A. J., & Tanvir, N. R. 2020a, ApJ, 895, 58
Gompertz, B. P., Nicholl, M., Schmidt, P., Pratten, G., & Vecchio, A. 2022a, MNRAS, 511, 1454
Gompertz, B. P., Cutter, R., Steeghs, D., et al. 2020b, MNRAS, 497, 726
Gompertz, B. P., Ravasio, M. E., Nicholl, M., et al. 2022b, arXiv:2205.05008
Gruber, D., Goldstein, A., Weller von Ahlefeld, V., et al. 2014, ApJS, 211, 12
Hu, R.-C., Zhu, J.-P., Qin, Y., et al. 2022, ApJ, 928, 163
Just, O., Bauswein, A., Ardevol Pulpillo, R., Goriely, S., & Janka, H. T. 2015, MNRAS, 448, 541
Kasen, D., Metzger, B., Barnes, J., Quataert, E., & Ramirez-Ruiz, E. 2017, Natur, 551, 80
Kasliwal, M. M., Nakar, E., Singer, L. P., et al. 2017, Sci, 358, 1559
Kasliwal, M. M., Anand, S., Ahumada, T., et al. 2020, ApJ, 905, 145
Kawaguchi, K., Kyutoku, K., Shibata, M., & Tanaka, M. 2016, ApJ, 825, 52
Kawaguchi, K., Shibata, M., & Tanaka, M. 2020, ApJ, 889, 171
Kilpatrick, C. D., Foley, R. J., Kasen, D., et al. 2017, Sci, 358, 1583
Korobkin, O., Rosswog, S., Arcones, A., & Winteler, C. 2012, MNRAS, 426, 1940
Kouveliotou, C., Meegan, C. A., Fishman, G. J., et al. 1993, ApJL, 413, L101
Kumar, P., & Zhang, B. 2015, PhR, 561, 1
Kyutoku, K., Fujibayashi, S., Hayashi, K., et al. 2020, ApJL, 890, L4
Kyutoku, K., Ioka, K., Okawa, H., Shibata, M., & Taniguchi, K. 2015, PhRvD, 92, 044028
Lamb, G. P., & Kobayashi, S. 2018, MNRAS, 478, 733
Lamb, G. P., Lyman, J. D., Levan, A. J., et al. 2019, ApJL, 870, L15
Lan, L., Lu, R.-J., Lü, H.-J., et al. 2020, MNRAS, 492, 3622
Lattimer, J. M. 2012, ARNPS, 62, 485
Lattimer, J. M., & Schramm, D. N. 1974, ApJL, 192, L145
Lattimer, J. M., & Schramm, D. N. 1976, ApJ, 210, 549
Lazzati, D., Perna, R., Morsony, B. J., et al. 2018, PhRvL, 120, 241103
Lei, W.-H., Zhang, B., & Liang, E.-W. 2013, ApJ, 765, 125
Lei, W.-H., Zhang, B., Wu, X.-F., & Liang, E.-W. 2017, ApJ, 849, 47
Li, L.-X., & Paczyński, B. 1998, ApJL, 507, L59
Li, L.-X., & Paczyński, B. 2000, ApJL, 534, L197
Li, Y., Zhang, B., & Lü, H.-J. 2016, ApJS, 227, 7
Liu, T., Gu, W.-M., & Zhang, B. 2017, NewAR, 79, 1
Liu, T., Liang, E.-W., Gu, W.-M., et al. 2012, ApJ, 760, 63
Lovelace, G., Duez, M. D., Foucart, F., et al. 2013, CQGra, 30, 135004
Lü, H.-J., Yuan, H.-Y., Yi, T.-F., et al. 2022, ApJL, 931, L23
Lyman, J. D., Lamb, G. P., Levan, A. J., et al. 2018, NatAs, 2, 751
MacFadyen, A. I., Woosley, S. E., & Heger, A. 2001, ApJ, 550, 410
Mandel, I., & Broekgaarden, F. S. 2022, LRR, 25, 1
Mandel, I., & Smith, R. J. E. 2021, ApJL, 922, L14
Margutti, R., Berger, E., Fong, W., et al. 2017, ApJL, 848, L20
Mei, A., Banerjee, B., Oganesyan, G., et al. 2022, arXiv:2205.08566
Metzger, B. D., Arcones, A., Quataert, E., & Martínez-Pinedo, G. 2010a, MNRAS, 402, 2771
Metzger, B. D., Martínez-Pinedo, G., Darbha, S., et al. 2010b, MNRAS, 406, 2650
Minaev, P. Y., & Pozanenko, A. S. 2020, MNRAS, 492, 1919
Mooley, K. P., Deller, A. T., Gottlieb, O., et al. 2018, Natur, 561, 355
Narayan, R., Paczynski, B., & Piran, T. 1992, ApJL, 395, L83
Narayana Bhat, P., Meegan, C. A., von Kienlin, A., et al. 2016, ApJS, 223, 28
Nasa High Energy Astrophysics Science Archive Research Center (Heasarc) 2014, HEAsoft: Unified Release of FTOOLS and XANADU, Astrophysics Source Code Library, record, ascl:1408.004
Nitz, A. H., Kumar, S., Wang, Y.-F., et al. 2021, arXiv:2112.06878
Norris, J. P., & Bonnell, J. T. 2006, ApJ, 643, 266
Norris, J. P., Cline, T. L., Desai, U. D., & Teegarden, B. J. 1984, Natur, 308, 434
Novikov, I. D., & Thorne, K. S. 1973, in Black holes (Les astres occlus), ed. C. DeWitt & B. DeWitt (New York: Gordon and Breach), 343
Paczynski, B. 1986, ApJL, 308, L43
Paczynski, B. 1991, AcA, 41, 257
Page, K. L., Evans, P. A., Tohuvavohu, A., et al. 2020, MNRAS, 499, 3459
Perego, A., Radice, D., & Bernuzzi, S. 2017, ApJL, 850, L37
Pian, E., D'Avanzo, P., Benetti, S., et al. 2017, Natur, 551, 67
Planck Collaboration, Aghanim, N., Akrami, Y., et al. 2020, A&A, 641, A6
Proga, D., & Zhang, B. 2006, MNRAS, 370, L61
Rastinejad, J. C., Gompertz, B. P., Levan, A. J., et al. 2022, arXiv:2204.10864
Rees, M. J. 1988, Natur, 333, 523
Román-Garza, J., Bavera, S. S., Fragos, T., et al. 2021, ApJL, 912, L23
Rosswog, S. 2007, MNRAS, 376, L48
Ruiz, M., Paschalidis, V., Tsokaros, A., & Shapiro, S. L. 2020, PhRvD, 102, 124077
Sagués Carracedo, A., Bulla, M., Feindt, U., & Goobar, A. 2021, MNRAS, 504, 1294
Sari, R., Piran, T., & Narayan, R. 1998, ApJL, 497, L17
Savchenko, V., Ferrigno, C., Kuulkers, E., et al. 2017, ApJL, 848, L15
Shao, Y., & Li, X.-D. 2021, ApJ, 920, 81
Shapiro, S. L. 2017, PhRvD, 95, 101303
Siegel, D. M., & Metzger, B. D. 2017, PhRvL, 119, 231102
Smartt, S. J., Chen, T. W., Jerkstrand, A., et al. 2017, Natur, 551, 75
Sun, H., Zhang, B., & Li, Z. 2015, ApJ, 812, 33
Sun, H., Liu, H.-Y., Pan, H.-W., et al. 2022, ApJ, 927, 224
Symbalisty, E., & Schramm, D. N. 1982, ApL, 22, 143
The LIGO Scientific Collaboration, the Virgo Collaboration, the KAGRA Collaboration, et al. 2021, arXiv:2111.03634
Troja, E., Piro, L., van Eerten, H., et al. 2017, Natur, 551, 71
Troja, E., Piro, L., Ryan, G., et al. 2018, MNRAS, 478, L18
Tsvetkova, A., Frederiks, D., Lysenko, A., et al. 2022, GCN, 31544, 1
Tunnicliffe, R. L., & Levan, A. 2012, in IAU Symp. 279, Death of Massive Stars: Supernovae and Gamma-Ray Bursts, ed. P. Roming, N. Kawai, & E. Pian (Cambridge: Cambridge Univ. Press), 415
von Kienlin, A., Meegan, C. A., Paciesas, W. S., et al. 2014, ApJS, 211, 13
von Kienlin, A., Meegan, C. A., Paciesas, W. S., et al. 2020, ApJ, 893, 46
Waxman, E., Ofek, E. O., & Kushnir, D. 2022, arXiv:2206.10710
Woosley, S. E., & Bloom, J. S. 2006, ARA&A, 44, 507
Wu, X.-F., Hou, S.-J., & Lei, W.-H. 2013, ApJL, 767, L36
Xiao, S., Zhang, Y.-Q., Zhu, Z.-P., et al. 2022, arXiv:2205.02186
Xie, X., Zrake, J., & MacFadyen, A. 2018, ApJ, 863, 58
Yang, B., Jin, Z.-P., Li, X., et al. 2015, NatCo, 6, 7323
Yang, J., Zhang, B. B., Ai, S. K., et al. 2022, arXiv:2204.12771
Yang, Y.-S., Zhong, S.-Q., Zhang, B.-B., et al. 2020, ApJ, 899, 60
Zaninoni, E., Bernardini, M. G., Margutti, R., & Amati, L. 2016, MNRAS, 455, 1375
Zhang, B. 2018, The Physics of Gamma-Ray Bursts (Cambridge: Cambridge Univ. Press)
Zhang, B. 2019, FrPhy, 14, 64402
Zhang, B., & Mészáros, P. 2001, ApJL, 552, L35
Zhang, B., & Mészáros, P. 2002, ApJ, 571, 876
Zhang, B., Zhang, B.-B., Liang, E.-W., et al. 2007, ApJL, 655, L25

Zhang, B., Zhang, B.-B., Virgili, F. J., et al. 2009, ApJ, 703, 1696
Zhang, B. B., Zhang, B., Sun, H., et al. 2018, NatCo, 9, 447
Zhang, H.-M., Huang, Y.-Y., Zheng, J.-H., Liu, R.-Y., & Wang, X.-Y. 2022, ApJL, 933, L22
Zhu, J.-P., Wu, S., Qin, Y., et al. 2022, ApJ, 928, 167
Zhu, J.-P., Wu, S., Yang, Y.-P., et al. 2021a, ApJ, 921, 156
Zhu, J.-P., Yang, Y.-P., Liu, L.-D., et al. 2020, ApJ, 897, 20
Zhu, J.-P., Wu, S., Yang, Y.-P., et al. 2021b, ApJ, 917, 24